Available online at www.sciencedirect.com

SCIENCE DIRECT®

Marine Chemistry 97 (2005) 14–33

MARINE CHEMISTRY

www.elsevier.com/locate/marchem

Photochemical production of hydrogen peroxide and methylhydroperoxide in coastal waters

Daniel W. O'Sullivan [a,*], Patrick J. Neale [b], Richard B. Coffin [c], Thomas J. Boyd [c], Christopher L. Osburn [c]

[a] *United States Naval Academy, Chemistry Department, 572 Holloway Road, Annapolis, MD 21402, USA*
[b] *Smithsonian Environmental Research Center, 647 Contees Wharf Road, Edgewater, MD 21037, USA*
[c] *Marine Biogeochemistry Section, Code 6114, US Naval Research Laboratory, Washington, DC 20375, USA*

Received 27 April 2004; received in revised form 5 April 2005; accepted 19 April 2005
Available online 13 September 2005

Abstract

Hydrogen peroxide (H_2O_2) has been observed in significant concentrations in many natural waters. Because hydrogen peroxide can act as an oxidant and reductant, it participates in an extensive suite of reactions in surface waters. Hydrogen peroxide is produced as a secondary photochemical product of chromophoric dissolved organic matter (CDOM) photolysis. Apparent quantum yields for the photochemical production of hydrogen peroxide were determined in laboratory irradiations of filtered surface waters from several locations in the Chesapeake Bay and in Arctic coastal waters with varying levels of CDOM. The apparent quantum yield for H_2O_2 decreases by about an order of magnitude from 280 nm to 500 nm, and the majority of H_2O_2 production occurs at wavelengths less than 340 nm. The apparent quantum yield for H_2O_2 production at 290 nm ranged from 4.2×10^{-4} to 2.1×10^{-6} mol H_2O_2 (mol photons)$^{-1}$ from freshwater to marine waters. A linear relationship was found between the production of H_2O_2 and change in CDOM absorbance characterized as photobleaching (loss of absorbance). No significant relationship was observed between DOC concentration and peroxide production. Methylhydroperoxide (CH_3O_2H) was the only short chain peroxide produced during the irradiations, and its production is at least an order magnitude less than that of hydrogen peroxide. Peroxide production was greatest in waters containing significant amounts of terrigenous C in the form of humic substances. Surface waters whose synchronous fluorescence spectra indicated the presence of polyaromatic and/or extensive conjugated compounds exhibited the greatest peroxide production. CDOM photobleaching is not significantly linked to apparent quantum yields for peroxide production.
2005 Published by Elsevier B.V.

Keywords: Hydrogen peroxide; Organic peroxides; Photochemistry; Seawater

1. Introduction

Hydrogen peroxide has been of interest since it was observed in significant concentrations in natural

* Corresponding author.
E-mail address: osulliva@usna.edu (D.W. O'Sullivan).

0304-4203/$ - see front matter. 2005 Published by Elsevier B.V.
doi:10.1016/j.marchem.2005.04.003

waters in the 1980s (Cooper and Zika, 1983). Because hydrogen peroxide can act as either an oxidant or a reductant, the suite of reactions involving hydrogen peroxide in natural waters is quite extensive. Hydrogen peroxide influences the redox chemistry of natural waters in several potentially important ways; by altering the speciation of trace metals in natural waters (Moffett and Zika, 1987), by changing the fate of pollutants, and potentially influencing the biological activity of the microbial community (Obernosterer et al., 2001). To fully characterize and model the effects of hydrogen peroxide and organic peroxides in natural waters, additional information regarding the mechanisms of production and loss in natural systems is needed, in particular the factors influencing the photochemical production of peroxides, for example DOC concentration, humic acid or fulvic acid content.

Appreciable levels of hydrogen peroxide have been observed in all types of natural surface waters. Cooper and Zika (1983) observed levels of hydrogen peroxide in different freshwater lakes and ground waters ranging from 10 s to 100 s of nanomolar. Zika et al. (1985) and Miller and Kester (1994, and references therein) have observed levels of hydrogen peroxide in surface ocean waters up to several hundred nanomolar. Levels of H_2O_2 of 10 to 100 μM have been observed in atmospheric aqueous phases: rainwater, cloud water, and fog waters (Zika et al., 1982; Schwartz, 1984). Peroxides in atmospheric aqueous phases are of interest because of their role in dissolved SO_2 oxidation. Hydrogen peroxide is believed to be the dominant oxidant for SO_2 in atmospheric aqueous phases with pH < 5 (Calvert et al., 1985). Although the presence of organic peroxides is often considered, there have been only a few observations of aqueous phase organic peroxide levels in natural waters. Sauer et al. (1997) observed 800 nM of hydroxymethyl hydroperoxide ($HOCH_2O_2H$) and 400 nM 1-hydroxyethyl hydroperoxide ($CH_3CH(OH)OOH$) in rainwater collected in the marine boundary layer off the coast of France. The sources of atmospheric aqueous phase peroxides are in situ photochemical generation and partitioning of gas phase peroxides into aqueous phases. The latter mechanism is supported by a large number of gas phase atmospheric peroxide observations. A variety of different analytical methods and field results involving gas phase peroxide observations have been reviewed by Lee et al. (2000, and references therein). Surface and aircraft-based programs have demonstrated that H_2O_2 is the dominant gas phase peroxide in the troposphere. The most abundant organic peroxides are CH_3OOH and hydroxymethylhydroperoxide (HMHP, $HOCH_2OOH$). CH_3OOH is the dominant organic peroxide in the remote marine troposphere (Heikes et al., 1996; O'Sullivan et al., 1999), and HMHP is thought to be more prevalent over continental regions (Hewitt and Kok, 1991; Tremmel et al., 1994; Weinstein-Lloyd et al., 1998).

A number of studies have determined the photochemical production of H_2O_2 in freshwater and ground waters (Cooper et al., 1988, 1994, Scully et al., 1996). Zuo and Hoigne (1992) examined the formation of H_2O_2 in atmospheric water that results from iron(III)-oxalato complex photolysis. Although observations of H_2O_2 in surface seawaters are abundant, only a few studies have examined the wavelength dependence of H_2O_2 production (Moore et al., 1993; Andrews et al., 2000; Yocis et al., 2000), and apparently no studies have examined the wavelength dependence of organic peroxide formation in surface waters. An understanding of the wavelength dependence of photochemical reactions is important for determining how photochemical processes might vary with changing environmental conditions, such as enhanced UV irradiance due to depletion of stratospheric ozone, or alterations in the depth of the photic zone where photochemical processes might dominate other mechanisms of DOM turnover (Del Vecchio and Blough, 2002).

H_2O_2 formation in surface waters is initiated by the absorption of sunlight by dissolved organic matter (DOM). The fraction of the DOM pool that interacts with sunlight, referred to as chromophoric dissolved organic matter (CDOM), impacts the optical properties of surface waters. Photolysis of CDOM in surface waters leads to the destruction of chromophores, potentially influencing the optical transparency of some surface waters (Gao and Zepp, 1998). CDOM photolysis is coincident with the production of a variety of oxygen radical species (OH, O_2^-, HO_2 and RO_2) in surface waters. These reduced oxygen radical species can further influence the optical environment by directly effecting aquatic organisms and/or altering the redox state of metals. Absorption of ultraviolet radiation by CDOM generates an excited singlet

state, which produces an excited triplet state through intersystem crossing (Eqs. (1) and (2)).

$$^1\mathrm{CDOM} + h\upsilon\ (280-400\ \mathrm{nm}) \rightarrow {}^1\mathrm{CDOM}^* \quad (1)$$

$$^1\mathrm{CDOM} + h\upsilon(280-400\ \mathrm{nm}) \rightarrow {}^3\mathrm{CDOM}^* \ (\text{via intersystem crossing}) \quad (2)$$

The excited triplet state (^{3}CDOM*) reacts with molecular oxygen to form superoxide (O_2^-) and its conjugate acid (HO_2).

$$^3\mathrm{CDOM}^* + {}^3O_2 \rightarrow \mathrm{CDOM}^+ + O_2^- \quad (3)$$

Superoxide dismutates to produce hydrogen peroxide (H_2O_2) and oxygen (Eqs. (4) and (5)).

$$HO_2 + HO_2 \rightarrow H_2O_2 + O_2 \quad (4)$$

$$HO_2 + O_2^- + H_2O \rightarrow H_2O_2 + O_2 + OH^- \quad (5)$$

Of the reactive oxygen species in seawater, superoxide has been observed in the highest steady state concentrations: 10^{-9} to 10^{-8} M. H_2O_2 is long-lived relative to superoxide, and relatively stable, making it an ideal photochemical marker (Miller, 1994).

Photochemically formed organic radicals are expected to participate in reactions analogous to HO_2, resulting in the production of short chain organic peroxides, for example methylhydroperoxide (MHP). Kieber and Blough (1990) demonstrated the formation of carbon centered radials during the photochemically induced cleavage of α Keto acids and ketones in aqueous solutions. Carbon centered radicals can react with oxygen to form RO_2, leading to organic peroxide formation. Another possible path for the formation of short chain organic peroxides is the addition of singlet oxygen to alkenes. Riemer et al. (2000) determined the photochemical production rates for C_2–C_4 alkenes in a variety of surface waters. These processes are not expected to lead to high levels of organic peroxides; however, they do provide several possible mechanisms for the in situ formation of short chain organic peroxides in surface waters. In an effort to develop quantitative relationships between CDOM photochemical transformation, loss of absorbance or fluorescence, and peroxide production, we have begun work to characterize the photochemical production of H_2O_2 and short chain organic peroxides in surface seawaters with varying levels of CDOM.

2. Methods

2.1. Peroxide analysis

An analytical technique for the determination of gas phase hydroperoxide concentrations (Lee et al., 1995; Kok et al., 1995) was modified for work in surface waters. Although a number of more sensitive analytical methods are available for the determination of hydrogen peroxide in seawater (Miller and Kester, 1988; Yuan and Shiller, 1999), these methods do not differentiate between hydrogen peroxide and other short chain organic peroxides.

The mobile phase composition for the high performance liquid chromatographic (HPLC) technique of Lee et al. (1995) was modified by the addition of methanol for application to surface seawaters. A mobile phase composition of 95% 1.00×10^{-3} M H_2SO_4 and 5% methanol was used for the analysis. All other reagent concentrations were identical to those described by Lee et al. (1995). Type II horseradish peroxidase and *p*-hydroxyphenyl acetic acid (Sigma Chemical Co.) were used as received, as were potassium hydrogen phthalate and sodium hydroxide (Fisher Scientific, ACS Certified Reagent Grade).

Surface seawater samples collected in acid-cleaned glass or PFA Teflon vials were filtered through 0.20 μm Millipore® filters and either analyzed promptly or refrigerated for later analysis (see Section 2.6). The content of C_1 to C_2 peroxides in each sample was determined using the modified HPLC fluorometric method (Lee et al., 1995). C_1 to C_2 hydroperoxides were separated by reverse phase HPLC on a 5 μm Inertsil ODS-2 PEEK column (4.6 mm × 250 mm, Alltech) followed by a post column derivatization reaction that formed a fluorescent dimer. Peroxidase catalyzed dimerization of *p*-hydroxyphenyl acetic acid occurs in the presence of peroxy functional groups at elevated pH (i.e., pH ≥ 10). Formation of the fluorescent dimer is proportional to the concentration of a given hydroperoxide and resulted in an average precision of better than ± 8% for analysis of the C_1 to C_2 hydroperoxides in this study. The detection limits, defined as three times the standard deviation of the

blank, for the two short chain organic peroxides observed in this study were: 3.0×10^{-8} M H_2O_2 and 1.5×10^{-8} M MHP.

2.2. Compound synthesis and standardization

MHP was synthesized from 30% H_2O_2 (Sigma-Aldrich Co.) and dimethyl sulfate (Eastman Kodak, Rochester, NY) in the presence of potassium hydroxide as described by Lee et al. (1995). In the presence of strong base, HO_2^- will undergo nucleophilic addition to either methyl group of dimethyl sulfate. MHP was synthesized by mixing 10 mmol of dimethyl sulfate, 20 mmol of 30% H_2O_2 and 20 mmol of 40% KOH in a round bottom flask that was immersed in an ice bath. The reaction was subsequently initiated by slowly heating the mixture to 60 °C. The solution was maintained at 60 °C until bubble formation stopped. During the reaction N_2 was initially passed through the solution at 5 ml/min. N_2 flow was controlled with a flow meter (Cole–Palmer), and increased in 50 ml increments every 10 min to a maximum 500 ml/min near the reaction end point. The N_2 gas passed in series through the reaction flask and then through 50 ml of 18 MΩ Millipore® water in a West–Gaeke bubbler immersed in an ice bath to capture MHP. This procedure separates MHP from H_2O_2 as a result of the large difference in the MHP and H_2O_2 Henry's law constants (O'Sullivan et al., 1996). The resulting MHP solution has a concentration between 10^{-3} and 10^{-4} M, and is stable for about a year when stored at 4 °C in brown borosilicate glass bottles. MHP stock solutions were calibrated by reaction with iodide. Iodine liberated by the reaction was determined spectrophotometrically following the procedure of Banerjee and Budke (1964). H_2O_2 stock solutions were made by dilution of a 30–35% H_2O_2 solution obtained from Sigma-Aldrich. H_2O_2 stock solutions were calibrated by titration with Ce(IV), which was made directly from analytical reagent grade cerium ammonium nitrate, a primary standard (Skoog et al., 1996).

2.3. Absorbance, fluorescence and DOC measurements

Optical density (A_λ) measurements for CDOM were made on a Shimadzu 160 UV spectrophotometer from 230 nm to 700 nm with 1 or 10 cm path-length (l) cells. A_λ was then corrected for the absorption of pure water as a function of wavelength (λ) using low-DOC 18 MΩ Millipore® water and converted to absorption coefficients according to Kirk (1994),

$$a_{\mathrm{CDOM}(\lambda)} = 2.303 A_\lambda l^{-1} \tag{6}$$

CDOM absorption spectra were corrected for instrument drift, fine particle scattering, and the difference between refractive indices for Milli-Q and estuarine and seawater using the following equation (Johannessen et al., 2003):

$$a_{\mathrm{CDOM}}(\lambda) = a_0 \mathrm{e}^{-S\lambda} + C \tag{7}$$

where a_0, S (the spectral slope coefficient), and C were calculated by nonlinear least squares regression (which used a Gauss–Newton algorithm). The parameter C was an offset value, and was subtracted from the entire absorption spectrum.

Photobleaching of CDOM for the photolysis experiments was characterized as the average loss of absorbance (L_{avg}, m^{-1}) over the range of 280 to 500 nm (Osburn et al., 2001).

$$L_{\mathrm{avg}} = \frac{\sum_{\lambda=280}^{500} a_{\mathrm{CDOM}(\lambda)\mathrm{initial}} - a_{\mathrm{CDOM}(\lambda)\mathrm{final}}}{220} \tag{8}$$

Changes in CDOM over the course of the photolysis experiments were also characterized by determination of the CDOM synchronous fluorescence (SF). Synchronous fluorescence was measured with a Shimadzu RF-5301 spectrofluorometer. The excitation wavelength range was 236 to 600 nm, and emission wavelengths ranged from 250 to 614 nm, maintaining a 14 nm offset between excitation and emission wavelengths. Several corrections were applied to raw spectra in order to compare our results with those in the literature. First, a correction for the inner-filter effect of the sample's absorption of source and emitted light were made following Belzile et al. (2002) and McKnight et al. (2001). Second, we applied a correction for nonlinearity in both excitation intensity and emission intensity per Shimadzu instructions. Third, we normalized each corrected SF spectrum to the water Raman signal area to give SF in Raman units (nm^{-1}; Laurion et al., 1997; Stedmon et al., 2003).

Concentrations of dissolved organic carbon (DOC) were determined by high-temperature catalytic oxidation using a MQ1001 TOC analyzer (Shimadzu Instru-

ments Inc.). Samples were acidified to pH 2 and sparged with high-purity N_2 gas for 10 min before analysis. DOC concentration was calibrated with 0, 83, 417 and 833 μM C standards prepared from potassium hydrogen phthalate. The average error of replicate DOC measurements was 23 μM C.

2.4. Photolysis experiments

Rates of primary photochemical reactions depend on the rate of absorption of sunlight and the efficiency with which the absorbed light results in product formation. The latter is described with a wavelength dependent ratio of the moles of product formed (peroxide) divided by the moles of photons absorbed at a particular wavelength (λ). Since the exact mechanism of peroxide production is unknown, as well as the identity of the absorbing chromophore, the measured efficiency of production is an "apparent" quantum yield ($\phi_{app,\lambda}$).

$$\phi_{app,\lambda} = \frac{\text{rate of peroxide production}}{I_\lambda F_\lambda} \quad (9)$$

Peroxide production rates are in moles of peroxide L^{-1} s^{-1}, I_λ is the intensity of light in the photochemical cell in units of moles of photons L^{-1} s^{-1}, and F_λ is the fraction of photons absorbed at a particular wavelength in the photocell.

For all exposure experiments, we used a modified solar simulator system (the "photoinhibitron") described in detail elsewhere (Neale and Fritz, 2001). A 1000 W xenon arc lamp was used as the light source. A condenser was used to generate a diverging beam, so that a 20–30 cm wide area was illuminated at a distance of about 1 m from the lamp. The beam was reflected upward with a mirror into pre-cleaned 112 cm^3 quartz bottom cuvettes containing the water samples. The quartz-bottom cuvettes were washed with 10% HCl and rinsed extensively with Milli-Q water. The irradiated region was divided into eight polychromatic sections using 5×5 cm Schott series WG long-pass filters with nominal cut-offs (i.e., factory-rated wavelengths at which irradiance transmission is 50%) at 280, 295, 305, 320, 335, 345, 365 and 400 nm. The effective irradiance transmitted by each filter is presented in Fig. 1. Ninety milliliters of a given water sample was placed in each quartz cuvette, capped with black Teflon lids, and positioned in each filter region. The grid of quartz

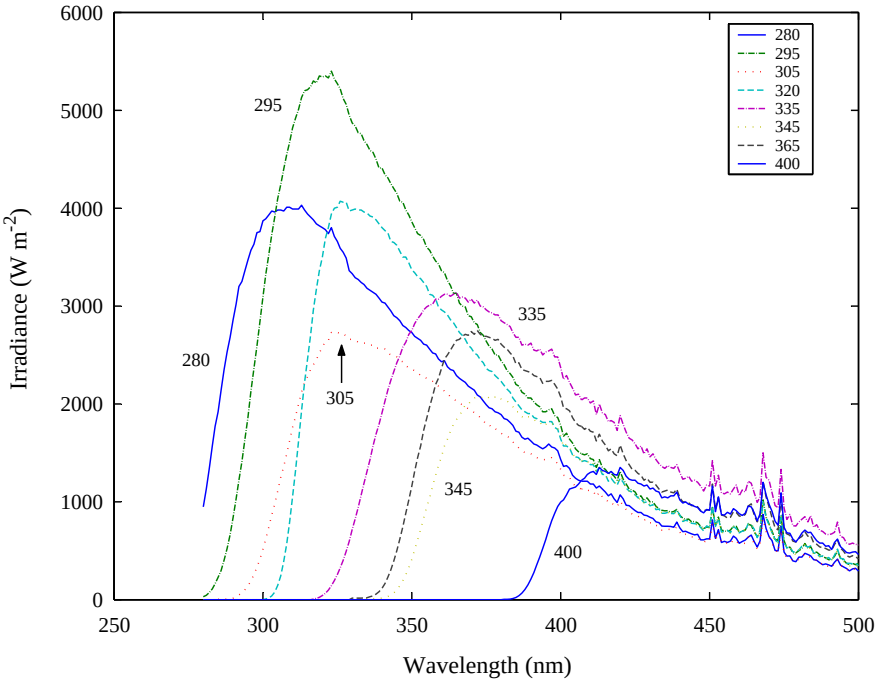

Fig. 1. Irradiance as a function of wavelength for the different filters used during the exposure experiments.

sample cuvettes was cooled with a fan to maintain a constant temperature (ca. 30 °C) during the irradiation experiment. An exposure experiment was run for 4 to 6 h.

Spectral irradiance (I_λ, mW m^{-2} nm^{-1}; 250–650 nm, 1 nm resolution) was measured under each filter using a custom spectroradiometer (Neale and Fritz, 2001). An NCL computer interface controlled scanning and performed data acquisition using the Spectrasense software package (Acton Research Co.). The system was calibrated for absolute spectral irradiance with a 1000 W NIST-traceable lamp (FEL), and a mercury arc lamp was used for wavelength offset corrections.

Spectral output of the xenon lamp and the spectral transmission of the cutoff filters determine the general spectral characteristics of the exposure system. Exposure level can be varied by several means. Different condenser positions change both the width of the beam, and the extent to which variation in output along the arc (i.e., higher output from the plasma ball just above the cathode) is imaged at the plane of illumination of samples. Relative spectral profile also varies along the arc, with higher UVA output from the plasma ball. Thus, beam intensity variations reflected with the mirror up through cutoff filters to the samples resulted in variable intensity through adjacent filters—especially those filters situated near the edge of the beam. Therefore, it was imperative that careful measurements of the spectral irradiance, modified by the long-pass filters, were made in each cuvette. Because the cuvettes were roughly similar in size to the long-pass filter, we had only one replicate per treatment. Spectroradiometer measurements were made at 5 locations in each cuvette (one measurement in each of the four corners and one measurement in the center) and the average value was used as the spectral irradiance for the sample.

Dissolved absorbance (a_{CDOM}, m^{-1}), CDOM synchronous fluorescence normalized to Raman units (nm^{-1}), and dissolved organic carbon (DOC) concentration (μM C) were measured in samples after irradiation and compared to dark-corrected initial results. The production of H_2O_2 and MHP were determined by measuring the difference in the concentrations of the species in samples before and after the irradiation experiment. Dark controls were also performed to account for any dark production of H_2O_2 and MHP.

2.5. Field sampling

Table 1 presents station data from all samples used in this study. Surface water samples for peroxide analysis and seawater for laboratory photolysis experiments were collected on several research cruises. The Chesapeake Bay samples were collected on the R/V Cape Henlopen during April 2001 (Spx 1), June 3–6th (2002) and September 3–6th 2002 (Spx 2–5). The Grizzly Bay sample (Spx 6) was collected from CTD casts in May 2002 on the R/V Point Sur. The Beaufort Sea sample (Spx 7) was collected by Dr. Warwick Vincent from CTD casts on the CCGS Pierre Radisson in October 2002. During the June cruise, surface seawater samples were collected periodically from the flowing seawater line on the R/V Cape Henlopen, filtered through a 0.22 μm PTFE syringe filter (Osmonics Inc.) and analyzed immediately. Samples were also collected from CTD casts during this cruise. During the September cruise, samples were collected from CTD casts and on-deck photolysis experiments. After filtration through 0.20 μm polysulfone filters (Gelman, PALL), these samples were refrigerated for subsequent laboratory analysis. Samples for photobleaching experiments were filtered through 0.20 μm polysulfone filters (Gelman, PALL) and stored in the dark at 4 °C.

2.6. Sample stability studies

Hydrogen peroxide concentrations in surface seawater are expected to range from 20 to 400 nM (Miller and Kester, 1994). Organic peroxides have not been observed in surface waters. Initial analytical work was performed to establish the capability of the analytical method to detect levels of peroxides in the range expected for natural waters. For natural waters the hydrogen peroxide detection limit is 30 nM and the MHP detection limit is 15 nM (three times the standard deviation of the blank). These detection limits are too high for determination of ambient levels in many surface waters. We have continued to optimize analytical procedures and decrease the detection limits for both hydrogen peroxide and MHP. The current analytical procedure is capable of quantifying changes in the concentration of hydrogen peroxide and MHP in laboratory photochemical experiments.

Table 1
Peroxide photolysis experiments

Experiment	Sample description	Date	Latitude	Longitude	Depth (m)	Temperature (°C)	Salinity	[DOC] (μM)	S (290–400) (m^{-1})	$a_{CDOM}(350)$ (m^{-1})	SF_{355}	$[H_2O_2]$ (nM)	[MHP] (nM)
SPx 1	Elizabeth River, VA	May-00	36°47.59′N	76°17.75′W	8.3	15.2	17.4	709	0.0167	3.37	18.93	4510[a]	280[b]
SPx 2	Susquehanna River, MD	Jun-02	39°47.59′N	76°01.96′W	3.0	24.2	0.1	203	0.0153	2.92	6.069	600	50
SPx 3	Estuarine, Chesapeake Bay	Jun-02	38°14.54′N	76°17.64′W	8.2	22.1	14	312	0.0172	2.92	5.852	440	15
SPx 4	Middle Atlantic Bight	Jun-02	37°05.46′N	75°31.04′W	9.8	19.5	33.1	63	0.0088	2.21	2.326	236	Nd
SPx 5	Middle Atlantic Bight	Jun-02	37°05.46′N	75°31.04′W	9.8	19.5	33.1	63	0.0088	1.72	5.94	290	Nd
SPx 6	Grizzly Bay, CA	Apr-01	38°03.54′N	121°47.88′W	3.0	16.9	0.4	475	0.0153	16.83	35.1	37	Bd
SPx 7	Beaufort Sea, Arctic	Oct-02	70°51.18′N	−133°39.00′W	2.0	−0.61	20.3	62	0.0192	1.15	6.564	385	Nd

Nd is none detected, Bd is below detection.
[a] Production at 280 nm, since the 305 sample was lost.
[b] Production at 295 nm, since the 305 sample was lost.

Samples for peroxide analysis of laboratory solar simulation experiments were stored in pre-cleaned glass vials with Teflon caps near 0 °C and kept in the dark until analysis. Decay of hydrogen peroxide in natural waters has been shown to follow first-order kinetics in freshwater and seawater (Cooper et al., 1994; Petasne and Zika, 1997). Peroxide decay occurs through a number of biologically mediated and chemically mediated pathways. In natural waters, particle-mediated decay dominates the removal of hydrogen peroxide (Cooper et al., 1994). The stability of peroxides in unfiltered surface waters was examined by determining peroxide loss rates in a brown acid-cleaned Nalgene® bottle. Loss of H_2O_2 and MHP followed first-order kinetics with half-lives of 120 and 45 min, respectively, at 24 °C in Chesapeake Bay surface waters with a salinity of 17.8‰. Our observed H_2O_2 half-life in unfiltered Chesapeake Bay surface waters is in good agreement with determinations by Cooper et al. (1994). For Bay waters, $t_{1/2}$ ranged from 2.49 to 12.2 h. The latter is similar to the 12.6 h half-life for unfiltered Vineyard sound surface waters observed by Moffett and Zafiriou (1990). Loss of MHP in surface waters is faster by nearly a factor of 3. The fast MHP loss rate may reflect a greater loss to the atmosphere due to its much lower solubility. A more extensive study of the processes that contribute to the loss of MHP in surface waters is needed to fully elucidate this difference.

Since the principal loss processes for H_2O_2 are particle-mediated, we examined the stability of H_2O_2 in 0.20 μm filtered samples (Osmonics Inc., PTFE syringe filters). The logistics precluded immediate analysis of peroxides during several of the cruises and for all of the laboratory irradiation experiments. Consequently, we examined the effects of sample storage on the peroxides. Samples were stored in pre-cleaned glass or PFA vials near freezing and kept in the dark for up to 20 days. H_2O_2 concentrations in 0.20 μm filtered seawater samples stored for 11 days were not statistically different (initially 139 ± 5 nM to 142 ± 4 nM, $n = 5$). No change was observed for H_2O_2 in seawater samples stored in either glass vials with Teflon tops or PFA vials for up to 20 days. MHP stored in glass vials decreased by 20% over the 20-day storage period. MHP concentrations in samples stored in the PFA vials increased by a factor of 2 over the storage period (initially 186 ± 8

nM to 360 ± 28 nM, $n = 5$). We have no viable explanation for the MHP increase in PFA vials. Freshwater samples did not exhibit the same stability during storage as seawater samples. Greater than 50% of both H_2O_2 and MHP were lost in glass and PFA vials stored for long periods. While all the freshwater samples had been frozen during storage, seawater samples did not freeze during storage, except for the Grizzly Bay sample that had a salinity of 0.4. Grizzly Bay is a shallow water system with high levels of trace metals. For example dissolved Cu and Mn concentrations were 35 and 900 nM, respectively, while particulate Cu and Mn concentrations in the water column were 9 and 200 nM, respectively (Beck et al., 2002). We speculate that compounds capable of degrading peroxides, for example iron, manganese and copper containing compounds, concentrate by exclusion during ice formation, resulting in rapid peroxide loss. Consequently, in future studies, our recommendation is that samples should be filtered, refrigerated and stored in glass vials, but not frozen. With these procedures the loss rate is sufficiently slow that peroxide loss is insignificant for short storage periods prior to analysis.

3. Results and discussion

3.1. Peroxide production

No dark production of H_2O_2 or MHP was observed in this work. The net production of the peroxides during irradiations is reported in Table 1 for selected cutoff filter treatments. Since the particle-mediated loss of peroxides in filtered surface waters is slow on the time scale of the irradiations (Section 2.5), the only other loss process would be direct photolysis of the peroxides. Moffett and Zafiriou (1990, 1993) determined H_2O_2 photolysis rates in surface seawater from Vinyard Sound, the Caribbean Sea and the Orinoco River and found that H_2O_2 photolysis was a small fraction (<5%) of the production rate. Photolysis rates for MHP in surface waters have not been determined. We anticipate MHP photolysis is also small relative to its production. Consequently, net peroxide production and gross production in the irradiation experiments are likely to be quite similar.

The Elizabeth River (VA), which drains the Dismal Swamp and has abundant CDOM ([DOC] = 709 μM C, a_λ[350 nm] = 15.04 m^{-1}), had H_2O_2 production rates (280–1130 nM h^{-1}) that were 10 times greater than those observed for other saline waters. H_2O_2 production in Elizabeth River water was similar to that of freshwater systems, such as Lake Ontario (160–1473 nM h^{-1}) and other temperate lakes (695–2120 nM h^{-1}) (Scully et al., 1996). Surface waters with substantial terrigenous run-off influence exhibited the greatest production of both H_2O_2 and MHP, with the majority of production occurring at wavelengths less than 320 nm. Only low salinity water produced MHP in substantial excess of the detection limit. We observed MHP production in surface seawater only in the June 2002 Chesapeake Bay estuarine sample at wavelengths less than 320 nm, and observed production rates were sufficiently close to the detection limit that the production uncertainty was large (2 ± 1 to 5 ± 1 nM h^{-1}). In both freshwater and seawater samples MHP production, where observed, was 10 to 20 times less than H_2O_2 production rates (Table 1).

The peroxide production from 295 nm to 400 nm for each surface water irradiation was summed and the relationship between the total peroxide production and the initial concentration of dissolved organic carbon was examined. Total H_2O_2 and total MHP production were well described by exponential functions of DOC concentration: ($[H_2O_2, nM] = 94.7e^{0.0056[DOC,\ \mu M]}$, $r^2 = 0.84$; $[MHP, nM] = 0.310e^{0.014[DOC,\ \mu M]}$, $r^2 = 0.77$). For both of the exponential relationships, data from the Grizzly Bay photolysis experiment was excluded. Grizzly Bay had an initial DOC concentration of 475 ± 12 μM, the second largest DOC concentration of the waters examined in this study. The total H_2O_2 production was 29 nM h^{-1}, and no MHP was observed in the Grizzly Bay sample. However, we suspect that the peroxides were produced but lost to decomposition processes during storage. The observed exponential dependences of production on [DOC] are entirely attributable to the high production of the Elizabeth River sample. For samples other than the Elizabeth River, there is no statistically significant relationship between peroxide production and [DOC]. Scully et al. (1996) observed a power relationship between H_2O_2 production and DOC content in freshwaters, similar to

that observed for the Elizabeth River sample. Whether relationships of this type should be extended to seawater systems is still unclear. More work is needed within the normal range of surface seawater DOC concentrations. If the dominant components responsible for peroxide production are terriginous in origin, a relationship between peroxide production and DOC content may not be significant for seawater systems.

Given the proposed mechanism for H_2O_2 production, where the photochemical production is initiated by CDOM photon absorption, one would expect a relationship between H_2O_2 production and CDOM. Many freshwater systems exhibit relationships between DOC content and/or absorbance, and H_2O_2 production (Scully et al., 1996). For our experiments, predominantly using surface seawaters, there is no clear relationship between H_2O_2 production and the mass-specific absorbance [a^* (m^2 μg C^{-1})=a_λ[350 nm] (m^{-1})/[DOC] (μg C m^{-3})] (Fig. 2). This suggests that H_2O_2 production in marine surface waters is more heavily dependent on the nature of the processes that follow CDOM photon absorption. Consequently, it appears that H_2O_2 production in marine surface waters is less dependent on the extent of CDOM absorption than is the case for freshwater systems. These results are consistent with earlier work in freshwaters which showed that more humic-rich freshwaters produced substantial amounts of H_2O_2. These results also indicate that more humic-rich waters promote MHP production. To our knowledge, these are the first data that show photochemical production of MHP in natural waters. The substantial production of peroxides from waters containing abundant terriginous C (humic substances) supports CDOM photon absorption as the induction step. However, in marine systems, competing reaction paths for the intermediates, or CDOM deactivation processes appear to reduce the peroxide yield.

3.2. CDOM property changes

The absorptivity as a function of wavelength for each of the surface water samples was determined before and after irradiation for each cutoff filter

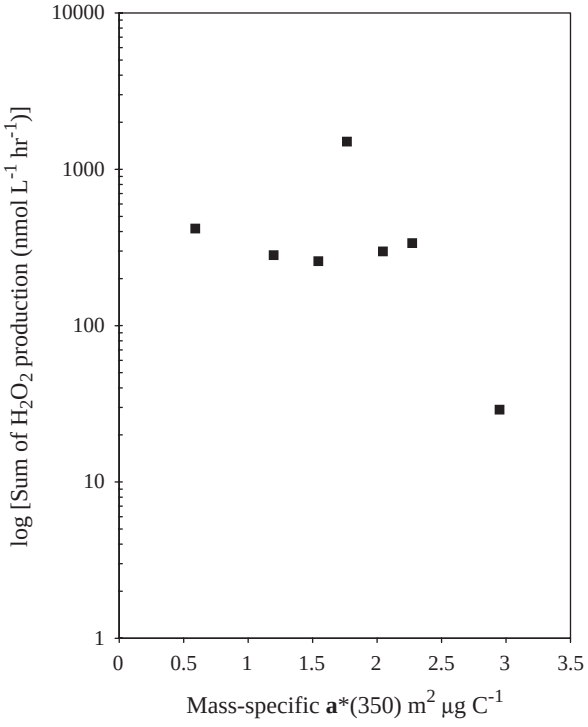

Fig. 2. The log of the sum of H_2O_2 production (■) during irradiations for the 295 nm to 400 nm cutoff filter exposures for each of the surface waters in the study versus the mass-specific absorbance.

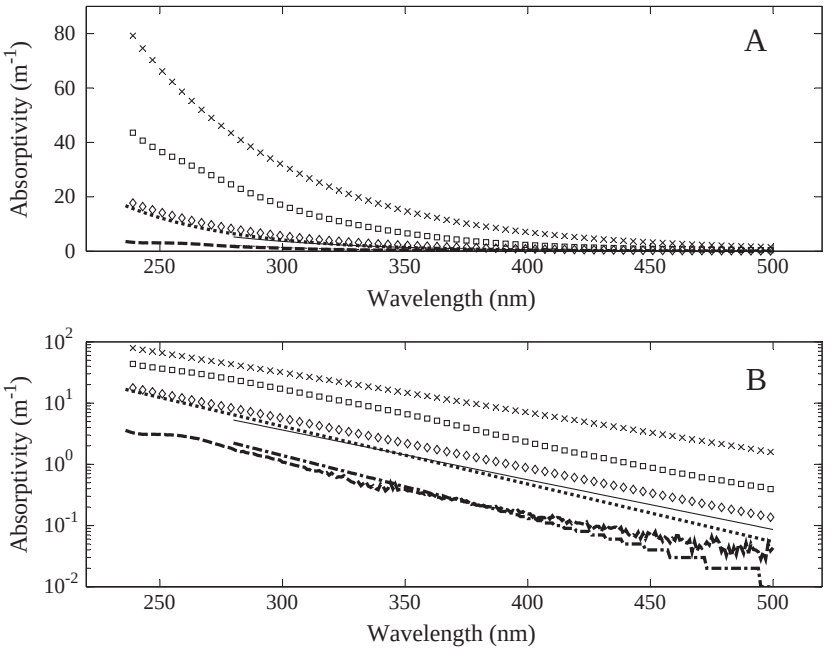

Fig. 3. (A) Absorptivity of various surface waters used in the irradiation experiments as a function of wavelenght, (×) Spx1, Elizabeth River; (□) Spx6, Grizzly Bay; (◇) Spx2, Freshwater Chesapeake Bay; (. . .) Spx3, Estuarine Chesapeake Bay; (—) Spx4, Marine Chesapeake bay; (-●-) Spx5, Marine Chesapeake Bay; (solid line) Spx7, Beaufort Sea Arctic surface waters. (B) Semolig plot of the absorptivities as a function of wavelength for each surface water sample.

treatment. The initial CDOM absorbance for each water sample is shown in Fig. 3. Absorptivities for the Chesapeake Bay waters were within the range of observations of earlier work (Rochelle-Newall and Fisher, 2002). Elizabeth river surface waters exhibited the greatest absorptivity at all wavelengths followed by Grizzly Bay surface waters (Fig. 3A). All surface water samples exhibited an exponential decrease in CDOM absorbance with increasing wavelength (Fig. 3B).

The loss of absorbance (photobleaching) that occurred over the course of each irradiation was characterized by calculating the average loss of absorbance in each optical filter treatment between 280 nm and 500 nm, L_{avg} (m^{-1}) (see Section 2.3). For all water samples, the greatest extent of photobleaching occurred in filter treatments with the most intense UV light exposure. A consistent relationship was found between L_{avg} (m^{-1}) and absorbed energy (J m^{-2}) summed over the same wavelength range that was used in the calculation of L_{avg}: more highly absorptive samples undergo greater photobleaching (Fig. 4). For all of the samples, loss of absorbance (photobleaching) exhibited a strong and remarkably similar dependence on the total absorbed energy. The dependence of photobleaching on absorbed energy indicates that bleaching is strongly dependent on the

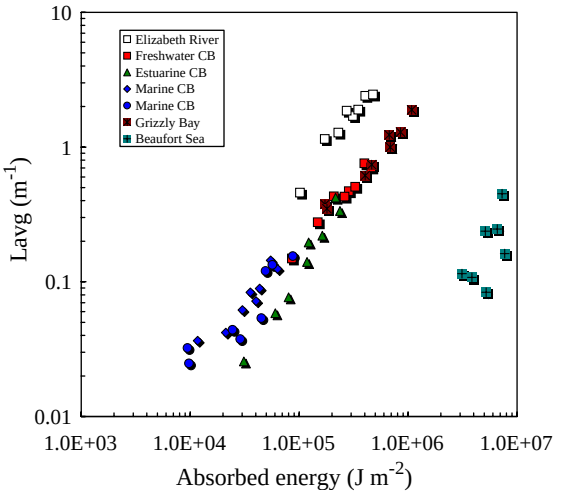

Fig. 4. Photobleaching in each cutoff filter treatment for the different surface waters as a function of absorbed energy.

absorbance spectrum of each sample. Since the irradiation spectrum was equivalent for all the surface waters, differences in the relationship between L_{avg} and absorbed energy are due to differences in both the quantum yield for photobleaching and the absorption spectra for various surface waters. Although the Elizabeth River and Beaufort Sea surface waters exhibit distinct relationships, the remaining waters all follow a similar trend. Consequently the products of the quantum yield for photobleaching and the absorption spectrum must be quite similar in the majority of these surface waters.

Elizabeth River and Grizzly Bay surface waters exhibited the strongest photobleaching in the 295 nm filter exposure, L_{avg} of 2.51 and 1.81 m^{-1}, respectively. Photobleaching for the Chesapeake Bay freshwater sample and the Beaufort Sea was 0.72 and 0.41 m^{-1}, respectively. Estuarine (Spx 3 at 295, L_{avg} 0.35 m^{-1}) and marine waters from the Chesapeake Bay(Spx 4 at 295, L_{avg} 0.14 m^{-1}, Spx 5, L_{avg} 0.15 m^{-1}) exhibited the smallest photobleaching response.

Changes in synchronous fluorescence (SF) spectra were examined as an additional approach to characterizing CDOM optical property changes. SF spectra obtained for each water sample prior to irradiation are shown in Fig. 5. Fluorophores containing one aromatic ring with aliphatic, alcoholic or ester linkages, isolated from a range of water types, usually exhibit a SF peak between 293 and 308 nm (Belzile et al., 2002, and references therein). Fluorophores with increased conjugation and substitution, and more polyaromatic systems shift the SF peaks to longer wavelengths. Initial SF spectra for both the Elizabeth River and Grizzly Bay surface waters exhibit broad peaks between 320 and 400 nm, broad features at wavelengths greater than 450 nm, and a clear humic peak at 570 nm (Fig. 5). The mid-wavelength range SF features are not present for the other surface waters, save for gently sloping shoulders. Freshwater and estuarine surface waters did exhibit some structure at wavelengths greater than 530 nm, though the intensity was greatly reduced. All surface waters exhibited SF features near 280 nm, although the magnitude and breadth of the features varied between samples. The SF spectra indicated the presence of monoaromatic, substituted carbon compounds in all surface waters. However, only the Grizzly Bay and Elizabeth River surface waters exhibited carbon com-

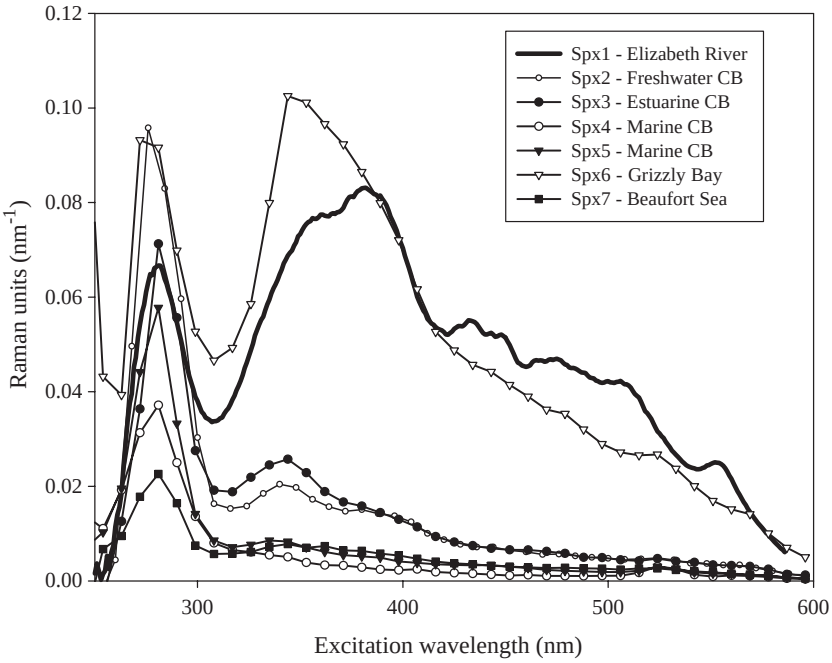

Fig. 5. Synchronous fluorescence spectra for each surface water sample, obtained with a 14 nm offset between excitation and emission scans.

pounds with polyaromatic character and/or extensive conjugation. The presence of these molecular features is consistent with the greater observed absorptivity of these surface waters.

We also measured changes in DOC concentration (presumed as photooxidation) during several of the experiments. However, after 5–6 h of irradiation, we did not find consistent decreases in DOC that would be indicative of photochemical oxidation of DOC to DIC. We suggest that photochemical CDOM oxidative and bleaching processes are decoupled.

3.3. Relationships between peroxide production and CDOM property changes

Since peroxide formation is a result of the photochemical excitation of CDOM (Eqs. (1)–(5)), one might expect a relationship between changes in CDOM optical properties and peroxide production. For freshwater systems, Scully et al. (1996) observed a linear relationship between H_2O_2 production and the initial absorption coefficient at 310 nm, as well as a linear relationship between H_2O_2 production and fluorescence. The relationship between H_2O_2 production and measures of CDOM property changes were examined over the course of our irradiations. Changes in CDOM were characterized by examination of changes in DOC concentrations during irradiation, and by examining loss of absorbance and changes in SF.

An observed linear relationship between H_2O_2 production and photobleaching, L_{avg} (H_2O_2 production (nmol L^{-1} h^{-1}) = 90.6 L_{avg} − 2.42, r^2 = 0.76), is shown in Fig. 6. The linear relationship is driven largely by the Elizabeth River results. In the absence of these data there is in no statistically significant relationship. H_2O_2 production in marine and estuarine waters is not strongly related to photobleaching. This may reflect the low concentrations of terrigenous C in these surface waters. These results are consistent with the lack of a relationship between peroxide production and mass-specific absorbance as discussed in Section 3.1. The SF spectra for the Elizabeth River surface water indicate the presence of polyaromatic compounds and extensive conjugation. These molecular features may be responsible for the bulk of H_2O_2 production. H_2O_2 production may prove to be a good proxy for the terrigenous C (humic content) of surface waters, although more work is needed to solidify this inference.

3.4. Wavelength dependence of peroxide production

The wavelength dependence of peroxide production was examined by determining the apparent quantum

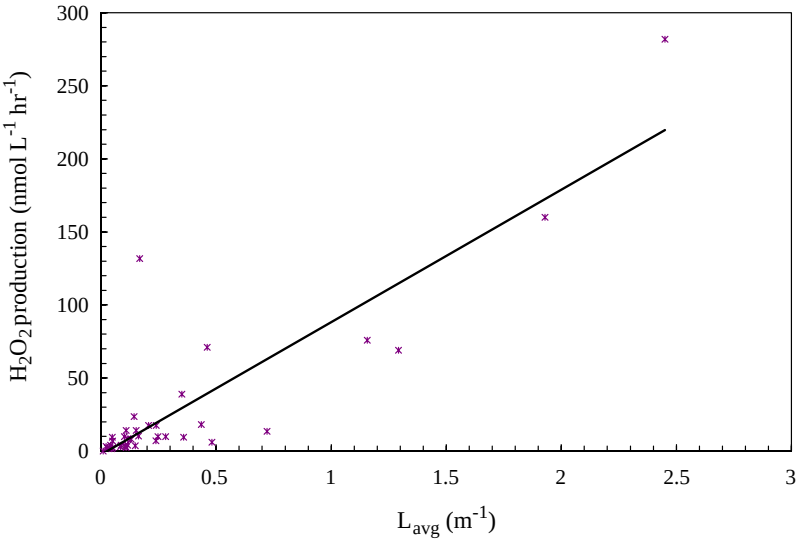

Fig. 6. Hydrogen peroxide production in each irradiated filter treatment for various surface waters versus photobleaching, L_{avg}, over the course of the irradiation.

yield ($\phi_{app,\lambda}$) for the production of H_2O_2 and MHP in the different surface waters. Due to the overlap in the irradiance field of adjacent filter treatments (Fig. 1)) a simple difference approach to determine apparent quantum yields was not possible. We employed a statistical curve fit method which used peroxide production values for each filter treatment and the absorbed energy measured under each filter to iteratively compute the best fit to the following equation:

$$W(\lambda) = \mathrm{W300} \times \mathrm{e}^{(-S_w[\lambda-300])} \quad (10)$$

$W(\lambda)$ is the spectral weighting function in mol H_2O_2 m^2 J^{-1}at λ, W300 is the function value at 300 nm, and S_w is the slope of the exponential. Best-fits to the spectral weighting equations were calculated using a Matlab® program that iteratively changed values for W300 and S_w to achieve the regression. Fits were performed using both the Gauss–Newton method and the Levenberg–Marquardt method. The results from both fitting methods were identical for all the water samples with the exception of Spx 7, Beaufort Sea surface waters (Table 2). For the Beaufort Sea surface waters, the statistical measure of the quality of the fit was similar for both methods, G–N, $r^2=0.80$ and L–M $r^2=0.77$. However, the slope generated by the G–N method ($S_w=0.0027$) was inconsistent with all other observations of the wavelength dependence of photochemical peroxide production. Consequently the L–M fit results were used for all subsequent calculations involving Spx 7. The resulting fits for the remaining surface waters had r^2 values in excess of 0.85 and are presented in Table 2 along with 95% confidence limits. This approach, calculation of a spectral weighting function (SWF) using the form of Eq. (10), is similar to prior studies that examined the wavelength dependence of absorption coefficients (Kirk, 1994; Vodacek et al., 1997; Osburn et al., 2001) and photochemical quantum yields for chemical species (Johannessen and Miller, 2001).

Using the resulting SWF, we calculated H_2O_2 production at each wavelength by multiplying the calculated $W(\lambda)$ by the absorbed energy ($E_a[\lambda]$). The resulting H_2O_2 production in mol H_2O_2 L^{-1} s^{-1} at each wavelength was divided by the photons absorbed at that wavelength in mol photons L^{-1} s^{-1}, generating $\phi_{app,\lambda}$ (Eq. (9)) at 1 nm intervals from 280 nm to 500 nm (Fig. 7). The limited production of MHP precluded statistically robust calculations of SWFs and apparent quantum yields for this compound. The apparent quantum yields for H_2O_2 production ranged from 4.2×10^{-4} to 6×10^{-7} mol H_2O_2 mol photons^{-1} for the different surface waters. For each surface water type, the $\phi_{app,\lambda}$ decreased with increas-

Table 2
Spectral weighting function fit parameters

Experiment	Description		Estimate	95% Confidence limits		R^2
				Upper	Lower	
SPx 1[a]	Elizabeth River, Nov. 2000	W300	1.329×10^{-5}	1.765×10^{-5}	8.922×10^{-6}	0.90
		Slope	−0.0075	−0.0017	−0.013	
SPx 2	Freshwater, June 2002 CB	W300	–	–	–	–
		Slope	–	–	–	
SPx 3	Estuarine water, June 2002 CB	W300	5.928×10^{-4}	7.098×10^{-4}	4.758×10^{-4}	0.92
		Slope	−0.0195	−0.0125	−0.0266	
SPx 4	Marine water, June 2002 CB	W300	9.205×10^{-4}	1.040×10^{-4}	8.012×10^{-4}	0.95
		Slope	−0.0039	−0.0016	−0.0062	
SPx 5	Marine water, CB	W300	5.538×10^{-3}	6.724×10^{-3}	4.351×10^{-3}	0.93
		Slope	−0.0047	−0.0005	−0.0090	
SPx 6	Grizzly Bay, May 2003	W300	8.226×10^{-5}	1.108×10^{-4}	5.378×10^{-5}	0.86
		Slope	−0.0105	−0.0035	−0.0175	
SPx 7[b]	Arctic 66, Marine	W300	1.056×10^{-5}	1.454×10^{-4}	6.586×10^{-5}	0.80
		Slope	−0.0010	0.0042	−0.0062	

[a] Multiply W300 by 1×10^{-6} to get molar H_2O_2 m^2 J^{-1}, all other are multiplied by 1×10^{-9}.
[b] The Levenberg–Marquardt fit and Gauss–Newton results were different for this sample, although the latter resulted in a better fit (r^2 =0.80), the L–M fit was used.

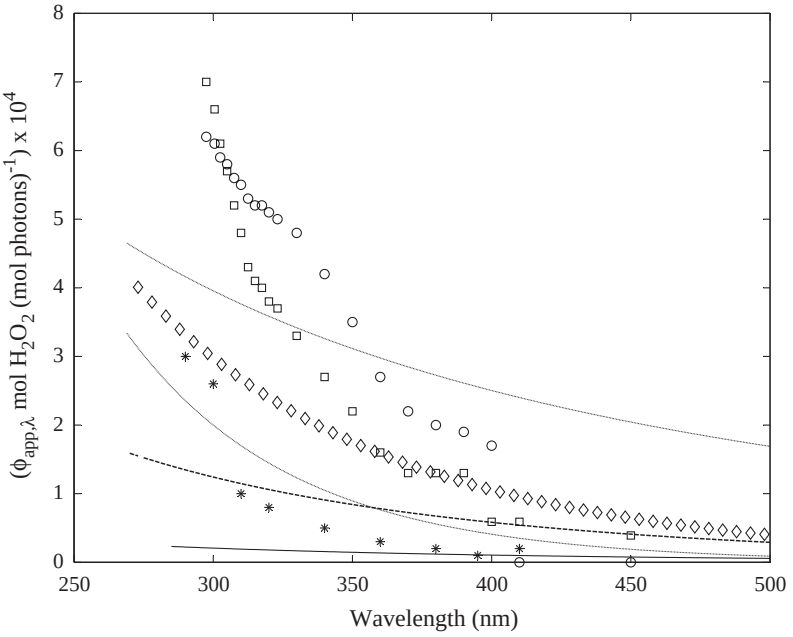

Fig. 7. Apparent quantum yield for H_2O_2 production as a function of wavelength, (◇) Spx1 Elizabeth River, (solid line) Spx4 Marine CB, and (dashed line) Spx5 Marine CB, results for the other surface waters are not graphical clarity. The dotted lines represent the 95% confidence limit for the Elizabeth River sample. The remaining symbols are AQY determinations from other work, (□) Cooper et al. (1988) NW Well 1 (ground water), and (○) VH Pond (surface freshwater), (∗) Yocis et al. (2000), Paradise Harbor (surface seawater).

ing wavelength, generally changing by an order of magnitude from 280 nm to 500 nm. For wavelengths less than 340 nm, the lowest quantum yields were observed for the Beaufort Sea surface waters (not shown). The observed $\phi_{app,\lambda}$ values for the Elizabeth River sample are similar to the range of apparent quantum yields observed by Cooper et al. (1988) at VH Pond Miami, FL, 7.0×10^{-4} to 5.9×10^{-5} (Fig. 7), and by Andrews et al. (2000) at the Shark River 1.19×10^{-3} to 1.7×10^{-4}. Observed $\phi_{app,\lambda}$ values in estuarine and marine waters are at the lower end of values obtained in marine surface waters influenced by the Orinoco River outflow (1.4×10^{-3} to 2.9×10^{-5}, Moore et al., 1993). The marine values are in good agreement with $\phi_{app,\lambda}$ observations by Yocis et al. (2000) for Antarctic surface waters (7.4×10^{-4} to 1.0×10^{-5}).

At any given wavelength, the values of $\phi_{app,\lambda}$ observed for the water types studied in this and other work, span at least an order of magnitude (Fig. 8). In addition, variations in the slope of the wavelength dependence are substantial and appear to be decoupled from water type. The slopes for Elizabeth River water, marine Chesapeake Bay waters, and Beaufort Sea surface waters are similar, as are the slopes for Grizzly Bay and estuarine Chesapeake Bay waters (Fig. 8). The range of values is larger than the uncertainty associated with the determinations, suggesting that there are differences in the photo-efficiency of H_2O_2 formation in different surface waters. There is a relationship between photobleaching and H_2O_2 production (see Section 3.3). However, the relationship seems to be robust only for freshwater systems. This implies that, in marine systems, the coupling of the reactions from CDOM excitation to peroxide formation is more tenuous. This could be the result of either more competitive superoxide reaction pathways than disproportionation and peroxide formation, or a lower content of "peroxide" producing chromophores in marine CDOM. For the same water samples, apparent quantum yields for peroxide production were substantially different than the apparent quantum yields (AQY) for CDOM photobleaching. A possible explanation for this difference is that changes in CDOM optical properties and changes in CDOM molecular composition (oxidation of CDOM and oxygen reduction) occur

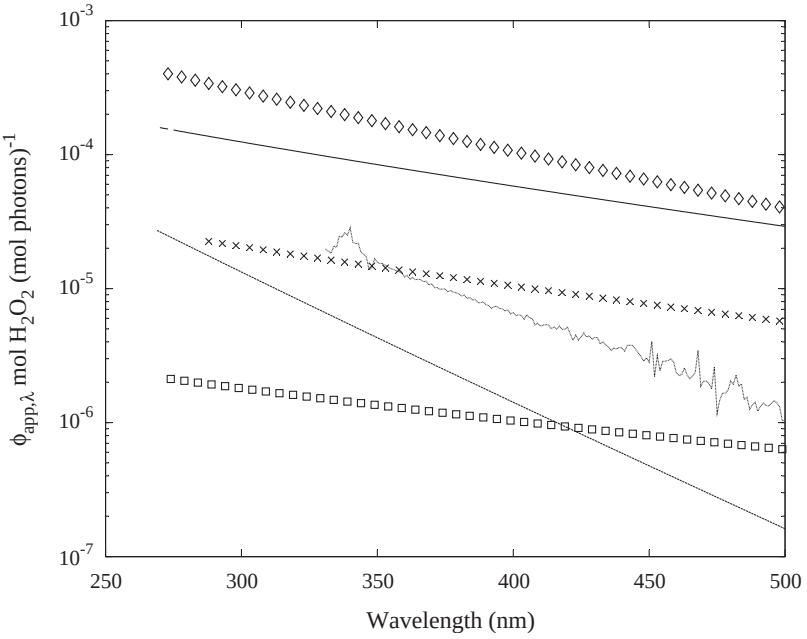

Fig. 8. Semilog plot of the apparent quantum yield for H_2O_2 production as a function of wavelength for the surface waters examine in the study; (◇) Spx1 Elizabeth River; (dashed line) Spx3 Estuarine CB; (×) Spx4 Marine CB; (solid line) Spx5 Marine CB; (dotted line) Spx6 Grizzly Bay; (□) Spx7 Beaufort Sea Arctic surface water.

along independent reaction paths. For example, one path may involve the photoxidation of a CDOM moiety leading to low molecular weight oxidation products and peroxide production, while other paths may not produce changes in CDOM molecular composition. For example, intramolecular conformation or configuration changes, or internal oxidation may result in absorbance loss without a change in molecular composition. Clearly more work is needed to elucidate the link between CDOM optical property changes and changes in chemical composition or conformation.

3.5. Wavelength dependence of photobleaching

Apparent quantum yields for photobleaching (AQY) were calculated for each surface water sample using procedures described by Osburn et al. (2001). Calculating photobleaching apparent quantum yields using the average loss of absorbance (L_{avg}), as in this work, sacrifices wavelength specific information. This approach makes it difficult to directly compare these AQYs to action spectra constructed from single wavelength responses using monochromatic radiation. In surface waters, changes to the dissolved absorbance spectrum occur under the influence of polychromatic radiation. In addition, this approach avoids uncertainties in characterizing the loss of absorbance in monochromatic action spectra as both "local" (loss of absorbance at the irradiation wavelength) and "global" (loss at other wavelengths) effects (Whitehead et al., 2000).

Substantial variation in AQY for photobleaching was observed (Fig. 9). In general, all AQY for marine waters exhibited small negative slopes with increasing wavelength while the estuarine and freshwaters had relatively steeper slopes. Our interpretation is that AQY provides a convenient way to examine the wavelength dependence of photobleaching for different CDOM samples. For example, steeper AQY slopes suggest a greater UV-B dependence for photobleaching than do shallower slopes. Although this is counter-intuitive given the large range in CDOM absorption among our samples (Table 1), it illustrates the variability in photoreactivity. Marine CDOM exhibited the highest photoreactivity per mol of absorbed photons per liter over the wavelength range between 280 and 500 nm.

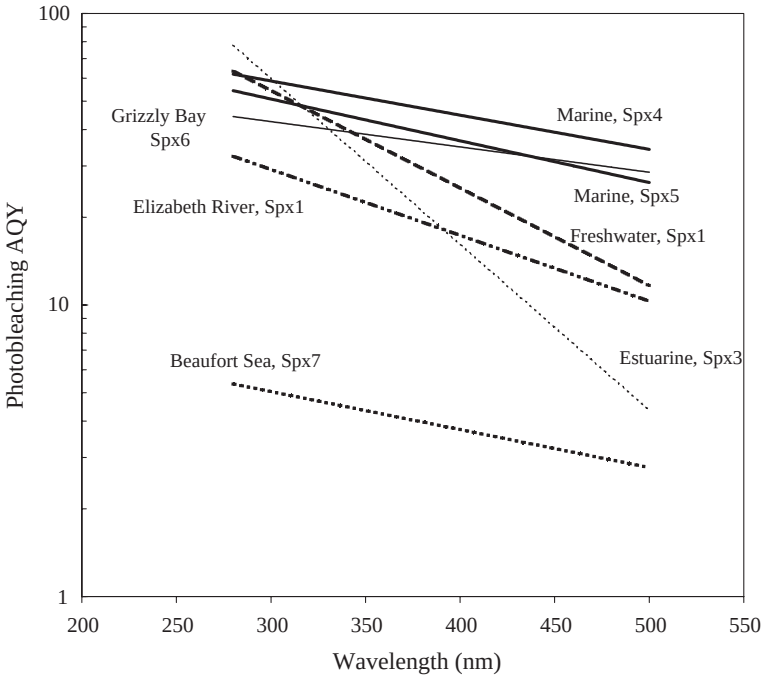

Fig. 9. Apparent quantum yield for photobleaching, measured as loss of absorbance (L_{avg}), as a function of wavelength for the various surface waters.

The AQY results for photobleaching suggest two fundamental insights into CDOM photoreactivity. First, the magnitude of AQY(λ) suggests a generally high photoreactivity given the number of photons absorbed by CDOM. Examination of Fig. 9 suggests that the Marine and Grizzly Bay CDOM were the most photoreactive. Second, slopes showing relatively weak variation with wavelength are possibly indicative of more extensive CDOM conjugation. The estuarine and freshwater CDOM clearly show the largest wavelength dependence, with UV-B values being nearly an order of magnitude greater than UV-A or blue light values. Vodacek et al. (1997) demonstrated that prior photobleaching of riverine water in the coastal ocean increases the spectral slope coefficient. By analogy, we expect that prior photobleaching may also increase the AQY slope, resulting in a greater UV-B dependence.

An initial examination of SF spectra supports the above conclusion. Fig. 10A shows the change in SF spectra for the Elizabeth River CDOM after an irradiation experiment. Qualitative loss of SF in the fulvic and humic regions of the spectrum are quite apparent and suggest substantial loss of terrestrial moieties due to sunlight. By comparison, for the Chesapeake Bay freshwater CDOM, Fig. 10B demonstrates much less loss of SF in those regions. Since, at present, these statements are only qualitative continuing work is needed to investigate the relationship between CDOM geochemistry (i.e., dissolved lignin concentrations) and AQY for photobleaching, photooxidation, and H_2O_2 production. An important conclusion drawn from the steeper slopes observed for the wavelength dependence of the photobleaching AQY in freshwaters and estuarine waters is that increases in UV-B radiation may lead to more significant photobleaching in these types of waters compared to marine waters.

3.6. Role of short chain organic peroxides in the electron balance

Andrews et al. (2000) used apparent quantum yields at 340 nm to examine the relationship between carbon oxidation and oxygen reduction pathways in surface waters. At 340 nm, the apparent quantum yield for H_2O_2 production is about 4×10^{-4}, and

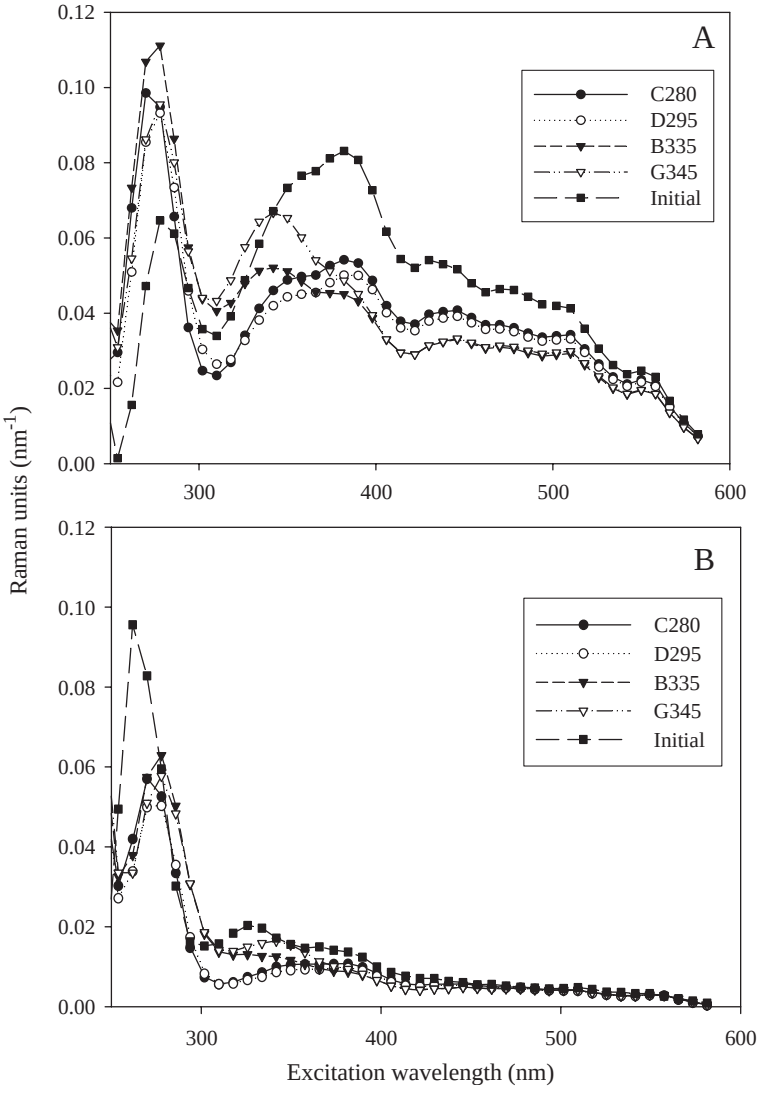

Fig. 10. Change in the synchronous fluorescence spectra upon irradiation for (A) the Elizabeth river sample, and (B) the freshwater sample from Chesapeake Bay. The Initial is prior to irradiation, and the remaining curves represent the different cutoff treatments as in Fig. 1.

the oxygen loss quantum yield is about 9×10^{-4} (Andrews et al., 2000). Oxygen loss along a two-electron path produces H_2O_2, while four-electron reduction produces water. On the oxidation side, stable carbon products are also observed with net two-electron changes. By comparing the stoichiometry of these processes, Andrews et al. (2000) noted that about 45% of the oxygen loss is via two electrons producing H_2O_2 ($\phi_{\lambda \text{app O2 loss}}/\phi_{\lambda \text{app H2O2}} * 100$). The remaining oxygen loss is either along a four-electron path to water, or by two-electron paths generating RO_2H or RO_2R'. Although we were unable to calculate a robust quantum yield for MHP, our observations suggest an upper bound MHP quantum yield equal to about 2×10^{-5} at 340 nm. The analytical method is capable of separating and distinguishing C_1 and C_2 organic peroxides (Lee et al., 1995), but only MHP was observed as a product in the irradiations. Consequently it is unlikely that C_1 or C_2 organic peroxides are significant photochemical products in surface seawaters. In addition, C_1 and C_2 organic peroxides cannot contribute significantly to the electron balance

in surface water. The analytical approach we used for this work is not capable of quantifying longer chain organic peroxides. Given the large and complex nature of DOM, production of longer chain organic peroxides could be significantly more efficient.

4. Conclusions

Photochemical H_2O_2 production was examined in a variety of surface waters that have varying levels of chromophoric dissolved organic matter (CDOM). For samples obtained in the Elizabeth River, H_2O_2 production was linearly related to CDOM photobleaching. H_2O_2 production in marine waters was not related to photobleaching. Hydrogen peroxide is produced as a secondary photochemical product of CDOM photolysis. Apparent quantum yields for the photochemical production of hydrogen peroxide were determined in filtered surface waters from several locations in the Chesapeake Bay and Beaufort Sea coastal waters. The range of apparent quantum yields, and variations in the wavelength dependence of the quantum yields, suggests that H_2O_2 production is more closely coupled to CDOM excitation in freshwater systems than in marine systems. This may be due to larger fractions of terrigenous CDOM in freshwater systems, or the presence of more effective superoxide loss pathways in marine systems. MHP was the only significant short chain organic peroxide observed as a photochemical product of CDOM photolysis. MHP production was only significant in freshwater and, even in freshwater, had production rates at least an order of magnitude smaller than that of hydrogen peroxide. The analytical approach used in this work was not capable of quantifying longer chain organic peroxides. Given the large and complex nature of DOM, production of longer chain organic peroxides could be significantly more efficient.

Acknowledgements

We thank Dr. Warwick Vincent and the CASES2002 expedition for supplying the Beaufort Sea sample, and the crews of the R/V Point Sur and R/V Cape Henlopen. This research was supported by the Naval Academy Research Council and the Office of Naval Research grant number N0001403WR20156 to DWO and grant number N0001403WX21256 to CLO. The manuscript was improved by the contributions of two anonymous reviewers, we are grateful for their efforts.

References

Andrews, S.S., Caron, S., Zafiriou, O.C., 2000. Photochemical oxygen consumption in marine waters: a major sink for colored dissolved organic matter? Limnol. Oceanogr. 45 (2), 267–277.

Banerjee, D.K., Budke, C.C., 1964. Spectrophotometric determination of traces of peroxides in organic solvents. Anal. Chem. 36, 792–796.

Beck, N.G., Bruland, K.W., Rue, E.L., 2002. Short-term biogeochemical influence of a diatom bloom on the nutrient and trace metal concentrations in South San Francisco Bay microcosm experiments. Estuaries 25 (6A), 1063–1076.

Belzile, C., Gibson, J.A.E., Vincent, W.F., 2002. Colored dissolved organic matter and dissolved organic carbon exclusion from lake ice: Implications for irradiance transmission and carbon cycling. Limnol. Oceanogr. 47 (5), 1283–1293.

Calvert, J.G., Lazarus, A., Kok, G.L., Heikes, B.G., Walega, J.G., Lind, J., Cantrell, C.A., 1985. Chemical mechanism of acid generation in the troposphere. Nature 317, 27–35.

Cooper, W.J., Zika, R.G., 1983. Photochemical formation of hydrogen peroxide in surface and ground waters exposed to sunlight. Science 220, 711–712.

Cooper, W.J., Zika, R.G., Petasne, R.G., Plane, J.M.C., 1988. Photochemical formation of H_2O_2 in natural waters exposed to sunlight. Environ. Sci. Technol. 22, 1156–1160.

Cooper, W.J., Shao, C., Lean, D.R.S., Gordon, A.S., Scully, J.F.E., 1994. Factors affecting the distribution of H_2O_2 in surface waters. In: Baker, L.A. (Ed.), Advances in Chemistry SeriesAmerican Chemical Society, pp. 393–422.

Del Vecchio, R., Blough, N.V., 2002. Photobleaching of chromophoric dissolved organic matter in natural waters: kinetics and modeling. Mar. Chem. 78, 231–253.

Gao, H., Zepp, R.G., 1998. Factors influencing photoreactions of dissolved organic matter in a coastal river of the south-eastern United States. Environ. Sci. Technol. 32, 1156–1160.

Heikes, B.G., Lee, M., Bradshaw, J., Sandholm, S., Davis, D.D., Chameides, W., Rodriguez, H., Liu, S., McKeen, S., 1996. Hydrogen peroxide and methylhydroperoxide distributions related to ozone and odd hydrogen over the North Pacific in the fall of 1991. J. Geophys. Res. 101, 1891–1905.

Hewitt, C.N., Kok, G.L., 1991. Formation and occurrence of organic peroxides in the troposphere: laboratory and field observations. J. Atmos. Chem. 12, 181–194.

Johannessen, S.C., Miller, W.L., 2001. Quantum yield for the photochemical production of dissolved inorganic carbon in seawater. Mar. Chem. 76, 271–283.

Johannessen, S.C., Miller, W.L., Cullen, J.J., 2003. Calculation of UV attenuation and colored dissolved organic matter absorption

spectra from measurements of ocean color. J. Geophys. Res. 108 (C9) (Art. No. 3301).
Kieber, D.J., Blough, N.V., 1990. Determination of carbon-centered radicals in aqueous solution by liquid chromatography with fluorescence detection. Anal. Chem. 62, 2275–2283.
Kirk, J.T.O., 1994. Light and Photosynthesis in Aquatic Ecosystems, 2nd ed. Cambridge University Press, Cambridge.
Kok, G.L., McLaren, S.E., 1995. HPLC determination of atmospheric organic hydroperoxides. J. Atmos. Ocean. Technol. 12, 282–289.
Laurion, I., Vincent, W.F., Lean, D.R.S., 1997. Underwater ultraviolet radiation: development of spectral models for northern high latitude lakes. Photochem. Photobiol. 65, 107–114.
Lee, M., O'Sullivan, D., Noone, K.B., Heikes, B.G., 1995. HPLC method for the determination of H_2O_2, C_1 and C_2 hydroperoxides in the atmosphere. J. Atmos. Ocean. Technol. 12, 1060–1070.
Lee, M., Heikes, B.G., O'Sullivan, D.W., 2000. Hydrogen peroxide and organic hydroperoxide in the troposphere: a review. Atmos. Environ. 34, 3475–3494.
McKnight, D.M., et al., 2001. Spectrofluorometric characterization of dissolved organic matter for indication of precursor organic material and aromaticity. Limnol. Oceanogr. 46 (1), 38–48.
Miller, W.L., 1994. Recent advances in the photochemistry of natural dissolved organic matter. In: Heltz, G.R., et al., (Eds.), Aquatic Surface Photochemistry. CRC Press, pp. 111–128.
Miller, W.L., Kester, D.R., 1988. Hydrogen peroxide measurement in seawater by (*p*-hydroxyphenyl)acetic acid dimerization. Anal. Chem. 60, 2711–2715.
Miller, W.L., Kester, D.R., 1994. Peroxide variations in the Sargasso Sea. Mar. Chem. 48, 17–29.
Moffett, J.W., Zafiriou, O.C., 1990. An investigation of hydrogen peroxide chemistry in surface waters of Vineyard Sound with $H_2^{18}O_2$ and $^{18}O_2$. Limnol. Oceanogr. 35 (6), 1221–1229.
Moffett, J.W., Zafiriou, O.C., 1993. The photochemical decomposition of hydrogen peroxide in surface waters of the eastern Caribbean and Orinoco River. J. Geophys. Res. 98, 2307–2313.
Moffett, J.W., Zika, R.G., 1987. Reaction kinetics of hydrogen peroxide with copper and iron in seawater. Environ. Sci. Technol. 21, 804–810.
Moore, C.A., Farmer, C.T., Zika, R.G., 1993. Influence of the Orinoco river on hydrogen peroxide distribution and production in the eastern Caribbean. J. Geophys. Res. 98, 2289–2298.
Neale, P.J., Fritz, J.J., 2001. Experimental exposure of plankton suspensions to polychromatic ultraviolet radiation for determination of spectral weighting functions. In: Slusser, J., Herman, J.R., Gao, W. (Eds.), Ultraviolet Ground- and Space-Based Measurements, Models, and Effects, vol. 4482. SPIE-The International Society for Optical Engineering, San Diego, pp. 291–296.
Obernosterer, I., Ruardij, R., Herndl, G.J., 2001. Spatial and diurnal dynamics of dissolved organic matter (DOM) fluorescence and H_2O_2 and the photochemical oxygen demand of surface water DOM across the subtropical Atlantic Ocean. Limnol. Oceanogr. 46 (3), 632–643.
Osburn, C.L., Zagarese, H.E., Morris, D.P., Hargreaves, B.R., Cravero, W.E., 2001. Calculation of spectral weighting functions for the solar photobleaching of chromophoric dissolved organic matter in temperate lakes. Limnol. Oceanogr. 46 (6), 1455–1467.
O'Sullivan, D.W., Lee, M., Noone, B.C., Heikes, B.G., 1996. Henry's law constant determinations for hydrogen peroxide, methyl hydroperoxide, hydroxymethyl hydroperoxide, ethyl hydroperoxide, and peroxyacetic acid. J. Phys. Chem. 100, 3241–3247.
O'Sullivan, D.W., Heikes, B.G., Lee, M., Chang, W., Gregory, G.L., Blake, D.R., Sachse, G.W., 1999. Distribution of hydrogen peroxide and methylhydroperoxide over the Pacific and South Atlantic Oceans. J. Geophys. Res. 104, 5635–5646.
Petasne, R.G., Zika, R.G., 1997. Hydrogen peroxide lifetimes in sourth Florida coastal and offshore waters. Mar. Chem. 56, 215–225.
Riemer, D.D., Milne, P.J., Zika, R.G., Pos, W.H., 2000. Photoproduction of nonmethane hydrocarbons (NMHCs) in seawater. Mar. Chem. 71, 177–198.
Rochelle-Newall, E.J., Fisher, T.R., 2002. Chromophoric dissolved organic matter and dissolved organic carbon in Chesapeake Bay. Mar. Chem. 77, 23–41.
Sauer, F., Limbach, S., Moortgat, G.K., 1997. Measurements of hydrogen peroxide and individual organic peroxides in the marine troposphere. Atmos. Environ. 31 (8), 1173–1184.
Schwartz, S.E., 1984. Gas- and aqueous-phase chemistry of HO2 in liquid-water clouds. J. Geophys. Res. 89, 11589–11598.
Scully, N.M., McQueen, D.J., Lean, D.R.S., Cooper, W.J., 1996. Hydrogen peroxide formation: the interaction of ultraviolet radiation and dissolved organic carbon in lake waters along a 43–75°N gradient. Limnol. Oceanogr. 41 (3), 540–548.
Skoog, D.A., West, D.M., Holler, F.J., 1996. Fundamentals of Analytical Chemistry, 7th edition. Harcourt College Publishers, Orlando, FL.
Stedmon, C.A., Markager, S., Bro, R., 2003. Tracing dissolved organic matter in aquatic environments using a new approach to fluorescence spectroscopy. Mar. Chem. 82, 239–254.
Tremmel, H.G., Junkermann, W., Slemr, F., 1994. Distribution of organic peroxides during aircraft measurements over the northeastern United States. J. Geophys. Res. 99, 5295–5307.
Vodacek, A., Blough, N.V., Degrandpre, M.D., Peltzer, E.T., Nelson, R.K., 1997. Seasonal variation of CDOM and DOC in the Middle Atlantic Bight: terrestrial inputs and photooxidation. Limnol. Oceanogr. 42, 674–686.
Weinstein-Lloyd, J.B., Lee, J.H., Daum, P.H., Kleinman, L.I., Nummermacker, L.J., Springston, S.R., Newman, L., 1998. Measurements of peroxides and related species in the 1995 SOS Nashville study. J. Geophys. Res. 103, 22361–22373.
Whitehead, R.F., De Mora, S., Demers, S., Gosselin, M., Monfort, P., Mostajir, B., 2000. Interactions of ultraviolet-B radiation, mixing, and biological activity on photobleaching of natural chromophoric dissolved organic matter: a mesocosm study. Limnol. Oceanogr. 45, 278–291.
Yocis, B.H., Kieber, D.J., Mopper, K., 2000. Photoproduction of hydrogen peroxide in Antarctic Waters. Deep-Sea Res., I 47, 1077–1099.
Yuan, J., Shiller, A.M., 1999. Determination of subnanomolar levels of hydrogen peroxide in seawater by reagent-injection chemiluminescence detection. Anal. Chem. 71, 1975–1980.

Zika, R.G., Saltzman, E.S., Chameides, W.L., Davis, D.D., 1982. H_2O_2 levels in rainwater collected in South Florida and the Bahama Islands. J. Geophys. Res. 87, 5015–5017.

Zika, R.G., Moffett, J.W., Petasne, R.G., Cooper, W.J., Saltzman, E.S., 1985. Spatial and temporal variations of hydrogen peroxide in Gulf of Mexico waters. Geochim. Cosmochim. Acta 49, 1173–1184.

Zuo, Y., Hoigne, J., 1992. Formation of hydrogen peroxide and depletion of oxalic acid in atmospheric water by photolysis of iron(III)-oxalato complexes. Environ. Sci. Technol. 26, 1014–1022.